# Myocyte culture with decellularized skeletal muscle sheet with observable interaction with extracellular matrix

**Satoshi Nakada**
Juntendo University
**Yuri Yamashita**
Juntendo University Graduate School of Medicine
**Seiya Akiba**
Juntendo University Graduate School of Medicine
**Takeru Shima**
Gunma University
**Eri Arikawa-Hirasawa** ( ehirasaw@juntendo.ac.jp )
Juntendo University

**Method Article**

**Keywords:** decellularization, mechanical stress, microdevice, skeletal muscle, extracellular matrix

**Posted Date:** May 19th, 2022

**DOI:** https://doi.org/10.21203/rs.3.rs-1632356/v1

# Abstract

**Background**: In skeletal muscle, muscle fibers are highly organized and bundled within the basement membrane. Several microfabricated substrate models have failed to mimic the macrostructure of native muscle, including various extracellular matrix (ECM) proteins. Even in substrates coated with proteins consisting of skeletal muscle-specific ECM compositions extracted from skeletal muscle, the function of each ECM protein remains, but the structural features of the basement membrane are lost. Therefore, in this study, we used decellularized muscle tissue and mouse myoblasts C2C12. We developed and evaluated a system to analyze the interaction between native ECM and myocytes.

**Methods**: Chicken skeletal muscle was sliced into sheets and decellularized with 1% SDS solution, 0.1N NaOH solution, and 50% ethanol to prepare decellularized skeletal muscle sheets (DSMS). C2C12 was then seeded and differentiated on DSMS. Immunostaining for ECM molecules was performed to examine the relationship between myoblast adhesion status, myotube orientation, and collagen IV orientation. Survival of myotubes in long-term culture was also confirmed by calcein staining.

**Results:** Decellularization of sliced skeletal muscle created a flexible skeletal muscle ECM-derived culture substrate. C2C12 myoblasts adhered to scaffolds in the DSMS and developed adhesion plaques and filopodia. In addition, C2C12 myotubes showed orientation along with the ECM orientation within the DSMS. Furthermore, RT-PCR results showed that C2C12 myogenic differentiation was promoted on the DSMS since the expression levels of myoD, etc., were increased early. On the plastic dish, detachment of cells occurred from day 6 of differentiation, and few cells survived to day 12, but on DSMS, no detachment occurred even on day 12, allowing long-term culture.

**Conclusions:** This study reports a novel myocyte culture method using sheet-like ECM structures obtained by decellularization. Myoblasts adhered to the sheet according to the orientation of the ECM, and the direction of myotube formation could be controlled. This culture technique reproduces a cell culture environment that reflects the properties of living skeletal muscle and allows studies on the interaction between the ECM and myocytes.


# Background

Tissues in living organisms have an orderly cellular arrangement owing to the basement membrane made from the extracellular matrix (ECM) [1–3]. In skeletal muscles, muscle fibers are bundled within basement membranes (endomysium and perimysium) to form highly organized bundles [4–6], enabling them to perform mechanical functions. In addition, the muscle basement membrane supports myogenesis and myotube formation [7–9] and is also involved in mechanotransduction and mechanical stress tolerance [10,11].

Several models have been reported to control myotube alignment via topological cues using microfabrication techniques to reproduce aligned myofibers *in vitro* [12–20]. Aligned myotubes promoted differentiation by arresting the cell cycle and increasing myotube diameter and length [13,17,19]. These

studies suggest that alignment control of myotube via topological cues promotes myotube formation. However, the microfabricated substrate is composed of purified ECM protein and cannot ideally mimic the macrostructure containing multiple ECM proteins in skeletal muscles.

Besides the effect of the macrostructure, each ECM molecule in the basement membrane itself has a different effect on the cells: collagen IV (COL IV) and laminin are involved in cell adhesion and migration [7], laminin promotes myogenesis and indirect myotube fusion [8,9], and chondroitin sulfate inhibits differentiation [21,22]. Because each tissue has a tissue-specific ECM composition [23–25], the use of a coating substrate composed of native ECM that is extracted from skeletal muscles can mimic the skeletal muscle-specific ECM protein composition accurately [26–29]. In addition, the fusion index and myotube area increased when culturing myocytes on native ECM coating compared to collagen I (COL I) coating, suggesting that native ECM promotes myotube differentiation [26,27]. However, the extracted native ECM can lead to the loss of structural characteristics in the basement membrane.

To solve this problem, we focused on decellularization technology by which cellular components can be removed from biological tissues to obtain the ECM constructs [23]. The resulting decellularized products possess the ECM macrostructure, thereby allowing us to examine the effect of basement membrane structures on myocytes [30,31]. Previously, Jank et al. demonstrated a model that highly mimics skeletal muscles by regenerating mouse skeletal muscles via cultured cell inoculation into decellularized mouse skeletal muscles [32]; however, it is difficult to apply this method in various applications owing to its complexity. Therefore, in this study, we devised a novel myocyte culture method using a sheet-like substrate made from decellularized skeletal muscle. Our new *in vitro* model will enable the observation of the interaction between the basement membrane ECM and myocyte and their responsiveness to mechanical stress loading.

# Materials And Methods

### 1. Fabrication of decellularized skeletal muscle sheet (DSMS).

Sheet-like substrates DSMS were fabricated from decellularized skeletal muscle. The decellularization technique was a modified version of the technique proposed by Urciuolo et al. [33]. The commercially available chicken breast meat was purchased and shaped using a surgical knife, subsequently frozen at − 30°C for overnight (O/N). Then, the frozen meat was sliced (1 mm thickness) longitudinally to the orientation of the muscle fibers using an electric meat slicer (RSL-220, Remacom, Mishima, Shizuoka, Japan). The slices were then washed with sterile ultra-pure water containing 1% penicillin-streptomycin (P/S, Thermo Fisher Scientific, Waltham, MA) and 250 μg/mL amphotericin B (AmB, Thermo) for 1 h.

The solution used in all decellularization processes was four times the volumes of the initial weight of the meat slices and was subjected to reciprocal shaking (NR-3, TAITEC, Saitama, Japan) at 100 rotations per minute at room temperature. The slices were then washed with sterile 1% sodium dodecyl sulfate (SDS) solution for 50 h to remove cellular components, during which the 1% SDS solution was changed four times. Next, the remaining SDS in the sheets was removed by washing with sterile 0.01N NaOH solution

for 15 min, followed by washing five times with sterile 50% ethanol for 1 h each. The sheets were washed twice for 10 min with a sterile storage solution (PBS, 1% P/S, 250 µg/mL AmB). Finally, the sheets were trimmed into 2 cm square using surgical knives, and DSMSs were prepared. The prepared DSMSs were stored at 4°C in a sterile storage solution for short-term storage and at − 30°C in a sterile antifreeze storage solution (PBS, 65% v/v glycerol, 1% P/S, 250µg/mL AmB) for long-term storage. DSMS stored in antifreeze solution was brought back to room temperature and was washed twice with a storage solution for 10 min for further use.

In order to confirm the progress of decellularization, the time course of change in the amount of protein eluted in the decellularization solution and in the protein component remaining in the skeletal muscle sheets was measured. The amount of protein eluted in the decellularization solution was determined by collecting a portion of the solution 30 min after the decellularization solution was changed. Protein quantification was performed using a BCA protein quantification kit (Pierce BCA Protein Assay Kit, Thermo). The amount of eluted protein was calculated as the amount of eluted protein per minute. To determine changes in residual protein components in the skeletal muscle sheets, a portion of the sheets was collected during the decellularization process and homogenized in SDS sampling buffer (62.5 mM Tris-HCl (pH 6.8), 2% (w/v) SDS, 10% glycerol, and 0.01% (w/v) bromophenol blue 42 mM dithiothreitol). The extracted proteins were subjected to BCA protein quantification, and the equal amounts of proteins were subjected to electrophoresis by SDS-PAGE. The gels were then stained with Coomassie Brilliant Blue stain to visualize the protein bands and imaged with a gel imaging system.

DSMS was attached to the polydimethylsiloxane (PDMS) chamber (Strex, Osaka, Japan) prior to use for DSMS stretching tests and cell culture. DSMS was placed in a PDMS chamber in PBS, with the ECM in the DSMS aligned with the stretching direction of the chamber. Then, PBS was removed, and DSMS was semi-dried for 30 min in a 37°C humidified $CO_2$ incubator. After that, PBS was added to rewet DSMS. This step allowed DSMS to stick tightly to the chamber even during cell culture. DSMS's characteristic to stick to the chamber enabled the same culture operations as conventional.

Stretching tests were performed to confirm the properties of DSMS. Stretching was performed uniaxially and aligned with the orientation of the DSMS.

Manual stretching was applied to confirm that the DSMS would stretch to the same degree when stretched through the chamber. The chamber with DSMS was set on a manual stretching tool (100 − 10, Strex) and stretched at different ratios, and the length change of the DSMS was measured. Automatic stretching was applied to observe the tolerance of the DSMS to repetitive stretching. The chamber with DSMS was set in the automatic stretching system (1400-10-R5, Strex) and repeatedly stretched at 1 Hz for 3 hours at a 20% stretching ratio.

### 2. Cell culture.

Mouse skeletal myoblasts (C2C12) were growth cultured on a plastic dish in a growth medium (GM, Dulbecco's modified Eagle's medium (DMEM) (10313021, Thermo) supplemented with 20% fetal bovine

serum (26140-079, Thermo) and 1% P/S (Thermo)). Growth C2C12 was passed before reaching 80% confluence and used within 10 passages to prevent loss of myogenic differentiation ability. Differentiation of C2C12 into myotubes was inducted with differentiation medium (DM, DMEM supplemented with 2% donor horse serum (2921149, MP Biomedicals, Tokyo, Japan) and 1% P/S). Cells were cultured at humidified 37°C under 5% $CO_2$, with the medium replaced every other day.

### 3. Myoblast adhesion and myotube formation on DSMS or plastic dish.

The C2C12 cells prepared in plastic plates were detached using 0.25% trypsin-EDTA, then suspended in GM, and seeded at $4 \times 10^4$ cells/$cm^2$ on DSMS attached to the chamber or on plastic dishes. Then, C2C12 was allowed to grow for two days, and differentiation was promoted by replacing the medium with DM.

### 4. Fluorescent microscopic observation.

Fluorescent staining was performed to observe the state of myoblast adhesion and myotube formation. Myocytes on DSMS were fixed with 4% paraformaldehyde for 25 min, washed three times with PBS for 10 min each, and then permeabilized with 0.3% Triton X-100 in PBS for 10 min. Next, the tissues were washed three times with PBS for 10 min each and blocked with a blocking solution (1% gelatin in PBS) for 30 min at room temperature. The tissues were then incubated with primary antibody (rabbit anti-COL IV antibody, AB756P, Millipore, Billerica, MA, USA) at 4°C overnight. They were again incubated with secondary antibody Alexa Fluor 546 Goat Anti-Rabbit IgG (H + L; Thermo) for 1 h at room temperature and later at 4°C O/N with Hoechst 33342 and Alexa Fluor 488 conjugated phalloidin (Thermo). For better microscopic observability, myocytes on DSMSs were incubated in a tissue clearing reagent Sca*l*eS4 [40% (w/v) D-sorbitol, 10% (w/v) glycerol, 4 M urea, 15% DMSO in $H_2O$] for 30 min prior to microscopic observation [34].

Calcein staining was performed to observe myotube survival in long-term culture on DSMS and plastic dishes. After 6 and 12 days of differentiation, living myotubes were washed with FluoroBrite DMEM (Thermo) and incubated with FluoroBrite DMEM containing 10 μg/mL of calcein-AM (Dojindo Laboratories, Kumamoto, Japan) for 60 min at 37°C. The cells were then washed with FluoroBrite DMEM and observed under the fluorescence microscope.

A BZ-X700 (KEYENCE, Osaka, Japan) was used for microscopic observation, and multifocal images were acquired using the z-stack function. The images were analyzed using ImageJ software (National Institutes of Health, Bethesda, MD, USA) [35].

### 5. Semi-quantitative reverse transcriptional PCR.

The mRNA expression levels of myocytes on DSMS and plastic dishes were measured on day 1 of the growth phase and days 0, 3, 6, and 12 of the differentiation phase. The mRNA expression levels were determined by semi-quantitative reverse transcriptional (RT) -PCR. As per the manufacturer's instructions,

total RNA was extracted from myocytes on DSMS and plastic dish using Qiazol and RNeasy mini kit (74104, Qiagen, Hilden, Germany). Possible contamination of genomic DNA was degraded using DNase I (Takara Bio Inc., Shiga, Japan) treatment for 15 min at room temperature. 1000 ng of total RNA was used for reverse transcription primed with Oligo(dT) using an AffinityScript QPCR cDNA Synthesis Kit (600559, Agilent Technologies, Texas, USA). Then, RT-PCR was performed (EmeraldAmp PCR Kit, Takara). The primer sequences used in this study are listed in Table 1.

PCR products were electrophoresed using a 2% agarose gel and stained by SYBR Gold (Thermo).

Gels were then detected with a UV gel imager (Amersham Imager 600, GE Healthcare Bioscience, Piscataway, NJ, USA), and band intensities were quantified using ImageJ densitometry.

The quantified mRNA expression levels were corrected for GAPDH mRNA levels and normalized to the levels of myocytes on DSMS day 1 of the growth phase.

Table 1
Primer sequences used in semi-quantitative RT PCR.

| Gene | F-Primer | R-Primer |
|---|---|---|
| Myf5 | 5'-TGTATCCCCTCACCAGAGGAT-3' | 5'-GGCTGTAATAGTTCTCCACCTGTT-3' |
| MyoD | 5'-AGTGAATGAGGCCTTCGAGA-3' | 5'-CTGGGTTCCCTGTTCTGTGT-3' |
| Myogenin | 5'-ACCAGGAGCCCCACTTCTAT-3' | 5'-ACGATGGACGTAAGGGAGTG-3' |
| Desmin | 5'-TCTCCCGTGTTCCCT-3' | 5'-ATACGAGCTAGAGTGGCA-3' |
| MHC embryonic | 5'-TCCGACAACGCCTACCAGTT-3' | 5'-CCCGGATTCTCCGGTGAT-3' |
| MHC neonatal | 5'-CAGGAGCAGGAATGATGCTCTGAG-3' | 5'-AGTTCCTCAAACTTTCAGCAGCCAA-3' |
| GAPDH | 5'-ACTCCACTCACGGCAAATTC-3' | 5'-CCTTCCACAATGCCAAAGTT-3' |

**6. Statistical analysis.**

Statistical analysis was performed using a t-test for independent samples with unequal variance using the Prism 9 software (GraphPad Software, LaJolla, CA, USA).

# Results

# 1. Preparation and properties of DSMS

To confirm that decellularization was sufficient, we checked the time course of changes in the amount of protein elution into the decellularization solution and changes in the protein component in the skeletal muscle sheets. Figure 2a shows the time course of changes in the amount of protein eluted into the

decellularized solution during the decellularization process. The amount of protein eluted decreased as the decellularization treatment progressed, with little elution observed between 6 and 30 hours. This result indicates that the proteins of the cellular components were completely eluted by the decellularization treatment. Next, the changes in protein composition in skeletal muscle sheets as the decellularization process were checked. In Fig. 2b, the DSMS were sampled during the decellularization process, the protein in skeletal muscle sheets was extracted, and the same amount of extracted protein was electrophoresed by SDS-PAGE followed by CBB staining. The bands visualized by CBB differed markedly between lanes 1 h, 2 h, and 3 h and lanes 6 h, 30 h, and 50 h of the decellularization process. The bands observed in lanes 1 h, 2 h, and 3 h were considered skeletal muscle contractile proteins such as MHC (220 kDa), α-actin (42 kDa), and tropomyosin-1 (34.7 kDa). On the other hand, lanes 6 h, 30 h, and 50 h were thought to be ECM proteins COL1α1 (140 kDa), COL1α2 (129 kDa), and COL1β [36]. The results confirm that as the decellularization process progresses, cellular components such as skeletal muscle contractile protein in skeletal muscle sheets were removed, and ECM protein remained. These results indicate that 30 hours of decellularization was sufficient to remove cellular proteins from the skeletal muscle sheet and fabricate DSMS.

The properties of the DSMS obtained by this determined decellularization process were confirmed. Figure 2c shows the appearance of skeletal muscle sheets before and after decellularization; the transparency of sheets increased after decellularization. Furthermore, the horizontal orientation of the ECM was visually confirmed. Next, the stretching properties of DSMS were confirmed. Figure 2d shows a DSMS attached to a PDMS chamber—the direction of the sheet's ECM aligned with the direction of the chamber's extension. In Fig. 2e, the manual uniaxial stretching was performed, and the extension rate of the chamber was compared with that of the sheet. When the chamber was stretched at 12.8%, the sheets exhibited an average of 15.9% elongation. When the chamber was stretched at 26.4%, the sheets exhibited an average of 21.5% elongation. The chamber with DSMS was placed in an automatic stretching system and subjected to 3 hours of 1 Hz stretching at 20% elongation. During stretching application, the DSMS did not detach from the chamber. These results indicate that the DSMS has suitable properties for applying mechanical stress.

These results indicate that DSMS has the suitable properties to apply mechanical stretch to DSMS through the PDMS chamber because of its strong adhesion to PDMS and sufficient extensibility.

Preparation and properties of decellularized skeletal muscle sheets. **a** Change in the amount of protein eluted by the decellularization solution. **b** Change in the remaining protein in the skeletal muscle sheet. The remaining protein was extracted and visualized by SDS-PAGE and CBB staining. **c** Appearance of the sheet before and after decellularization. DSMS: the direction of the ECM remaining in the sheets can be visually confirmed. **d** DSMS attached to the chamber. **e** DSMS extension associated with manual stretching.

# 2. Morphology of myoblasts and myotubes on DSMS

Morphological observations were made to determine the effects of DSMS on myoblasts and myotubes. To confirm the difference in adhesion of C2C12 to DSMS and plastic dish, C2C12 was seeded into DSMS, and myoblast adhesion was compared in a plastic dish the next day. Then, the cells were stained for fiber actin with fluorescence conjugated phalloidin, followed by nuclear staining with Hoechst 33342 and immunostaining with anti-COL IV antibody. On the plastic plate, C2C12 exhibited a star-shape and irregular cell orientation (Fig. 3d), whereas, on DSMS, C2C12 cells were spindle-shaped and adhered in line with scaffolds (Fig. 3a). The adhesion along the decellularized structures was similar to that reported in previous studies [37]. Through detailed observation of cell adhesion, C2C12 on DSMS was observed to have multiple fiber actin spikes between the scaffolds, which were thought to be adhesion plaques. The adhesive plaques and the shape of the cells suggest that lamellipodia and filipodia are formed (Fig. 3b, c) [38,39].

In order to confirm the influence of DSMS on myotube formation, myotube differentiation was induced by changing to the differentiation medium. On DSMS, myotubes formed in the same direction as DSMS, and many myotubes formed in the ± 20° range, as shown in Fig. 3f and g, suggesting that the orientation of the myotubes is controlled by DSMS. On the other hand, on the plastic dish, myotubes formed in random directions, as shown in Fig. 3h and i.

Comparison of myoblasts and myotubes morphology. Green: phalloidin, red: COL IV, and blue: Hoechst 33342. **a** Myoblasts adhered to DSMS. Myoblasts aligned with the remaining COL IV in DSMS. **b**: Magnified image. Myoblasts on DSMS developed actin spikes that appeared to be adhesion plaques (arrow). **c**: Magnified image. Myoblasts on DSMS developed lamellipodia and filipodia (arrow). **d** Myoblast adhered to the plastic dish. **e** Magnified image. Myoblasts on plastic dishes do not develop adhesive spots. **f** Myotube formation on DSMS. Myotube formed along with the ECM orientation in DSMS. **g** Histogram of angles in myotube formed on DSMS. Most myotubes were in the ± 20 ° range. **h** Myotube formation on the plastic plate. Myotube on a plastic formed in random orientation. **i** Histogram of angles in myotube formed on the plastic plate. Various angles of myotubes were present on the plastic plate.

### 3. Myocyte differentiation on the DSMS.

RT-PCR was performed from mRNA extracted from myocyte seeded on DSMS and plastic dish (Fig. 4). The earliest myogenic regulatory factor (MRF) Myf5 expression was higher in DSMS throughout the entire culture period [40,41]. MyoD, an MRF involved in myoblast proliferation and early differentiation, was higher expressed in G0 of DSMS [41,42]. Myogenin, an MRF involved in myotube fusion, was highly expressed in D0 of DSMS [41,43,44]. There was no significant difference in desmin expression between DSMS and plastic dishes. Expression of embryonic and neonatal MHC was higher in DSMS at D0 [45–47]. These results indicate enhancement of myogenic regulatory factor expression and accelerated expression of immature MHC.

G1, Growth 1 day. D0–D12, differentiation 0–12 days. The numbers above the bands indicate the band intensities determined by densitometry. Each band intensity was corrected by the GAPDH band intensity

value and then normalized by the DSMS G1 value.

**4. Myotube viability on the DSMS.**

In order to observe myotube cell survival on DSMS and plastic plates during long-term culture, viable cells were stained with calcein. On Day 6 of differentiation, myotubes on both DSMS and plastic dishes were stained with calcein, indicating that myotubes were formed and survived on each substrate (Fig. 5a, c). However, on Day 12, the number of myotubes stained with calcein on the plastic dish decreased, suggesting cell detachment occurred (Fig. 5d). On the other hand, myotubes on DSMS survived without detachment even on Day 12 of differentiation (Fig. 5b) and were still alive 24 days after differentiation (data not shown).

# Discussion

In this study, longitudinally sliced skeletal muscle was decellularized to obtain flexible substrates suitable for myocyte culture. This allowed us to control the alignment of myoblast adhesion and myotube formation, promote myocyte differentiation, and suppress myotube detachment, enabling a long-term culture of myotubes.

# Properties of DSMS

The decellularization process resulted in a sheet-like structure with only the skeletal muscle ECM remaining. As a result of shaping the ECM so that the alignment of skeletal muscle fibers could be seen before decellularization, the alignment of the ECM was maintained after decellularization. The sheets also had strong adhesion to the PDMS chamber, high flexibility of the sheets, and high durability to withstand prolonged stretching stimuli. This is not only a great advantage in normal cell culture operations but also makes it possible to apply mechanical stretching stimuli through the sheet.

**Myoblast adhesion and Myotube formation on the DSMS.**

Aligned myofiber is a major characteristic of skeletal muscle. Therefore, many studies have been conducted to align myoblasts and myotubes in order to create *in vitro* models that mimic skeletal muscle. In this study, we observed the effect of skeletal muscle ECM-derived scaffolds on myoblast morphology, confirming that myoblasts formed multiple adhesion plaques and elongated filopodia along ECM scaffolds. Because adhesion plaque explores the topology of the scaffold, more adhesion plaque is required on complex surface structures [48]. The multiple adhesion plaque formed by C2C12 myoblasts on DSMS suggests that myoblasts on DSMS are actively interacting with the complex scaffold of DSMS. Furthermore, myoblasts on DSMS were observed to extend filopodia along the DSMS scaffold. During migration, cells form filopodia in the direction of migration and adhere to the scaffold. The cells then translocate toward the scaffold formed by the filopodia by actomyosin-based contraction forces [38,39]. Therefore, C2C12 was considered to be migrating along with the orientation of the DSMS scaffold

because C2C12 was forming filopodia along with the orientation of the DSMS scaffold. Since DSMS affects C2C12 migration, DSMS could be used as a material for studies on myoblast migration.

This study also succussed that myotubes form along the alignment of the DSMS ECM. On the plastic dish, myotubes were formed in a random orientation, whereas on the DSMS, myotubes were formed in a direction ± 20˚ of the DSMS orientation. A possible mechanism by which myotube orientation is regulated by DSMS is that the scaffold in DSMS influences myotube orientation. Cells are influenced by topographical cues [49], and culture systems have been developed to control myotube orientation by creating microgrooves on the culture plate or through the linear pattern of ECM coating [12,17–20]. Similarly, DSMS shows a micro-groove-like 3D structure along with the sheet orientation. Therefore, it is possible that this groove-like structure controlled myotube orientation.

It is also possible that adhesion and the migration pattern of C2C12 myoblasts on DSMS affect myotube orientation. On the plastic dish, C2C12 cells migrate freely on the uniform dish surface and come in contact with the surrounding cells randomly, leading to fusion [50]. As a result, C2C12 on the plastic dish can form myotubes randomly. On the other hand, on DSMS, myoblasts adhere along with the fibrillar collagen, as shown in Fig. 3. Since the fibrillar collagen structure in DSMS has a consistent directionality, the migration direction of myoblasts may be restricted. Therefore, it is suggested that myotubes are formed along the DSMS alignment due to myoblast contact and fusion occurring on the DSMS fibrous collagen scaffold.

The ability to control myotube orientation on the DSMS via DSMS orientation is a very advantageous feature for mechanical stimulation; the alignment of myotube orientation on the DSMS allows mechanical stimulation to be applied at an accurate extension rate along the long myotube axis.

This may allow for a more detailed study of the intensity of the mechanical stimulus and the response of the cell.

### Myocyte differentiation on the DSMS.

Several proteins in the ECM of skeletal muscle basement membrane have affected myogenic differentiation.

Laminin promotes myoblast adhesion [7] myogenesis [8] and also indirectly promotes myoblast fusion by increasing cell-to-cell affinity [9]. COL IV promotes myoblast adhesion and migration [7]. On the other hand, chondroitin sulfate has been reported to inhibit differentiation [21,22]. Decellularized skeletal muscle is also expected to affect myogenic differentiation because the skeletal muscle basement membrane ECM remains. Previous studies have reported that solubilized decellularized skeletal muscle was used for coatings to promote myogenic differentiation [26–29]. Since the present study showed accelerated expression of myogenic regulatory factors and earlier expression of immature MHC, it is suggested that culture on DSMS promoted myogenic differentiation. This suggests that the effect of

differentiation-promoting ECMs such as Lam and COL IV is stronger than the inhibition of differentiation by chondroitin sulfate.

### Myotube viability on the DSMS.

Detachment of myotubes was frequently observed in long-term cultures and is caused by the disruption of adhesion as myotubes increase contractility with differentiation and maturation [12,51–56]. Since this detachment is a major limiting factor in research, detachment suppression methods have been studied [57,58]. In this study, we confirmed that the survival of myotubes on DSMS revealed that myotube detachment did not occur, and myotubes survived longer on DSMS than on plastic dishes.

One possible mechanism for the long-term survival of myotubes on DSMS without detachment is that myotubes may adhere more firmly to DSMS than to plastic dishes. As mentioned above, myoblasts formed multiple fiber actin spikes and adhered to DSMS, suggesting that myoblasts adhere more tightly to DSMS. Similarly, myotubes may adhere tightly to DSMS by forming abundant adhesion molecules. However, in a previous study, the adhesion force of myotubes to substrates was examined [53]. Among the substrates examined, the adhesion force to plastic dishes was the strongest, but the detachment of myotubes was observed on plastic dishes. Therefore, the adhesive strength of myotubes alone may not be sufficient to explain the mechanism by which myotubes do not detach and can be cultured in DSMS for long periods of time.

Another possible mechanism for the long-term viability of myotubes on the DSMS is that the low stiffness of the DSMS may prevent detachment of the myotubes. Previous studies have reported that substrate stiffness affects myotube detachment and survival during long-term culture [52,53]. Bettadapur et al. cultured myotubes on hard PDMS, which has the same stiffness as glass or plastic plates, and on soft PDMS, and a previous study reported that soft PDMS suppressed detachment of myotubes for one and three weeks [52]. The rigid substrate will not be able to absorb the spontaneous contractile force of the myotubes, causing the molecular adhesion to collapse and detachment. In contrast, the soft substrate is thought to absorb the contractile force and inhibit myotube detachment. Skeletal muscle stiffness, expressed as passive elasticity, is about 12 kPa and decreases slightly after decellularization [53,59]. The DSMS in this study is also expected to have a similar stiffness because it is a substrate obtained by decellularizing skeletal muscles. Therefore, the low stiffness of DSMS is considered to have inhibited myotube detachment.

Another possibility is that the time to detachment may have been prolonged simply because the time course of differentiation was extended. Thinner myotubes were observed in the DSMS on Day 6 than in the plastic dish (Fig. 6a, c), suggesting that culture on DSMS may have caused a delay in myotube differentiation. However, based on the semi-quantitative RT-PCR results, no significant difference exists in the expression of differentiation markers between DSMS and plastic dish, suggesting that the myotube differentiation time course on DSMS was not delayed. The thinner myotubes on DSMS maybe that myoblasts adhered to the fibrillar collagen scaffold, and migration and cell-cell contact were limited, thereby inhibiting excessive fusion.

These suggest that the main mechanism myotubes survived longer on the DSMS was not due to differences in the time course of differentiation but because of the firm adhesion of myotubes to the DSMS and the low stiffness of the DSMS prevented detachment. Using DSMS for myotube culture prevents myotube detachment and enables more prolonged cell culture. This property of DSMS-based culture could be a great advantage in studies using cultured myotubes.

## Conclusions

This study reports a novel myocyte culture method using sheet-like ECM structures obtained by decellularization. Myoblasts adhered to the sheet according to the orientation of the ECM, and the direction of myotube formation could be controlled. Furthermore, by applying mechanical stimulation to the myotubular cells in each sheet, we evaluated the mechanical stress resistance of the myocytes.

## Abbreviations

ECM extracellular matrix

DSMS decellularized skeletal muscle sheet

P/S penicillin-streptomycin

AmB amphotericin B

SDS sodium dodecyl sulfate

PBS phosphate-saline buffer

DMEM Dulbecco's modified Eagle's medium

## Declarations

# Ethics approval and consent to participate

Not applicable.

# Consent for publication

Not applicable.

# Availability of data and material

The datasets used and analysed during the current study are available from the corresponding author on reasonable request.

# Funding

This research was funded by Grant-in-Aid from JSPS KAKENHI (Grant Number 21K17589, 19K19951), and the Acceleration Program for Intractable Diseases Research utilizing Disease-specific iPS cells, which were granted by the Japan Agency for Medical Research and Development. Japanese Society for the Promotion of Science, grants in aid of Research into Rare and Intractable Diseases (H29-nanchitou(nan)-ippan-030) from the Ministry of Health, Labor, and Welfare of Japan, an Intramural Research Grant (2–5) for Neurological and Psychiatric Disorders from the National Center of Neurology and Psychiatry.

# Competing interests

The authors declare that they have no conflict of interest.

# Authors' contributions

Conceptualization, S.N., and E.A.; methodology, S.N.; software, S.N.; validation, S.N., Y.Y., and E.A.; formal analysis, S.N.; investigation, S.N., and T.S.; data curation, S.N., and T.S.; writing—original draft preparation, S.N.; writing—review and editing, Y.Y. and E.A.; visualization, S.N.; supervision, E.A.; project administration, E.A.; and funding acquisition, S.A. and E.A. All authors have read and agreed to the published version of the manuscript.

# Acknowledgements

We wish to thank Hidetoshi Sakurai for providing research opportunities and various consultations.

## References

1. Costa KD, Lee EJ, Holmes JW. Creating alignment and anisotropy in engineered heart tissue: Role of boundary conditions in a model three-dimensional culture system. Tissue Eng. 2003;9:567–77.
2. Foolen J, Van Donkelaar CC, Nowlan N, Murphy P, Huiskes R, Ito K. Collagen orientation in periosteum and perichondrium is aligned with preferential directions of tissue growth. J Orthop Res. 2008;26:1263–8.
3. Wojciech Pawlina MHR. Histology: A Text and Atlas: With Correlated Cell and Molecular Biology. 8th ed. Wolters Kluwer Health; 2018.

4. Sanes JR. The basement membrane/basal lamina of skeletal muscle. J Biol Chem [Internet]. Â© 2003 ASBMB. Currently published by Elsevier Inc; originally published by American Society for Biochemistry and Molecular Biology.; 2003;278:12601–4. Available from: http://dx.doi.org/10.1074/jbc.R200027200
5. Trotter JA, Purslow PP. Functional morphology of the endomysium in series fibered muscles. J Morphol. 1992;212:109–22.
6. Purslow PP. The Structure and Role of Intramuscular Connective Tissue in Muscle Function. Front Physiol. 2020;11.
7. Olivero DK, Furcht LT. Type IV collagen, laminin, and fibronectin promote the adhesion and migration of rabbit lens epithelial cells in vitro. Invest Ophthalmol Vis Sci [Internet]. 1993;34:2825–34. Available from: http://www.ncbi.nlm.nih.gov/pubmed/8360016
8. Foster RF, Thompson JM, Kaufman SJ. A laminin substrate promotes myogenesis in rat skeletal muscle cultures: Analysis of replication and development using antidesmin and anti-BrdUrd monoclonal antibodies. Dev Biol. 1987;122:11–20.
9. Lehka L, Rędowicz MJ. Mechanisms regulating myoblast fusion: A multilevel interplay. Semin Cell Dev Biol [Internet]. Elsevier; 2020;104:81–92. Available from: https://doi.org/10.1016/j.semcdb.2020.02.004
10. Humphrey JD, Dufresne ER, Schwartz MA. Mechanotransduction and extracellular matrix homeostasis. Nat Rev Mol Cell Biol [Internet]. Nature Publishing Group; 2014;15:802–12. Available from: http://www.nature.com/doifinder/10.1038/nrm3896
11. Csapo R, Gumpenberger M, Wessner B. Skeletal Muscle Extracellular Matrix – What Do We Know About Its Composition, Regulation, and Physiological Roles? A Narrative Review. Front Physiol. 2020;11:1–15.
12. Lam MT, Sim S, Zhu X, Takayama S. The effect of continuous wavy micropatterns on silicone substrates on the alignment of skeletal muscle myoblasts and myotubes. Biomaterials. 2006;27:4340–7.
13. Choi JS, Lee SJ, Christ GJ, Atala A, Yoo JJ. The influence of electrospun aligned poly(ε-caprolactone)/collagen nanofiber meshes on the formation of self-aligned skeletal muscle myotubes. Biomaterials. 2008;29:2899–906.
14. Bian W, Bursac N. Engineered skeletal muscle tissue networks with controllable architecture. Biomaterials [Internet]. 2009;30:1401–12. Available from: http://www.ncbi.nlm.nih.gov/pubmed/19070360
15. Zhao Y, Zeng H, Nam J, Agarwal S. Fabrication of skeletal muscle constructs by topographic activation of cell alignment. Biotechnol Bioeng [Internet]. 2009;102:624–31. Available from: https://www.ncbi.nlm.nih.gov/pmc/articles/PMC3624763/pdf/nihms412728.pdf
16. Altomare L, Gadegaard N, Visai L, Tanzi MC, Farè S. Biodegradable microgrooved polymeric surfaces obtained by photolithography for skeletal muscle cell orientation and myotube development. Acta

Biomater [Internet]. Acta Materialia Inc.; 2010;6:1948–57. Available from: http://dx.doi.org/10.1016/j.actbio.2009.12.040

17. Takahashi H, Shimizu T, Nakayama M, Yamato M, Okano T. The use of anisotropic cell sheets to control orientation during the self-organization of 3D muscle tissue. Biomaterials [Internet]. Elsevier Ltd; 2013;34:7372–80. Available from: http://dx.doi.org/10.1016/j.biomaterials.2013.06.033
18. Charest JL, García AJ, King WP. Myoblast alignment and differentiation on cell culture substrates with microscale topography and model chemistries. Biomaterials. 2007;28:2202–10.
19. Huang NF, Lee RJ, Li S. Engineering of aligned skeletal muscle by micropatterning. Am J Transl Res. 2010;2:43–55.
20. Evans DJR, Britland S, Wigmore PM. Differential response of fetal and neonatal myoblasts to topographical guidance cues in vitro. Dev Genes Evol. 1999;209:438–42.
21. Warita K, Oshima N, Takeda-Okuda N, Tamura JI, Hosaka YZ. Degree of suppression of mouse myoblast cell line C2C12differentiation varies according to chondroitin sulfate subtype. Mar Drugs. 2016;14.
22. Mikami T, Koyama S, Yabuta Y, Kitagawa H. Chondroitin sulfate is a crucial determinant for skeletal muscle development/regeneration and improvement of muscular dystrophies. J Biol Chem. 2012;287:38531–42.
23. Gilbert TW, Sellaro TL, Badylak SF. Decellularization of tissues and organs. Biomaterials. 2006;27:3675–83.
24. Lutolf MP, Hubbell JA. Synthetic biomaterials as instructive extracellular microenvironments for morphogenesis in tissue engineering. Nat Biotechnol. 2005;23:47–55.
25. Uriel S, Labay E, Francis-Sedlak M, Moya ML, Weichselbaum RR, Ervin N, et al. Extraction and assembly of tissue-derived gels for cell culture and tissue engineering. Tissue Eng - Part C Methods. 2009;15:309–21.
26. Choi Y-J, Park SJ, Yi H-G, Lee H, Kim DS, Cho D-W. Muscle-derived extracellular matrix on sinusoidal wavy surfaces synergistically promotes myogenic differentiation and maturation. J Mater Chem B [Internet]. 2018;6:5530–9. Available from: http://xlink.rsc.org/?DOI=C8TB01475B
27. DeQuach JA, Mezzano V, Miglani A, Lange S, Keller GM, Sheikh F, et al. Simple and high yielding method for preparing tissue specific extracellular matrix coatings for cell culture. PLoS One. 2010;5:1–11.
28. Stern MM, Myers RL, Hammam N, Stern KA, Eberli D, Kritchevsky SB, et al. The influence of extracellular matrix derived from skeletal muscle tissue on the proliferation and differentiation of myogenic progenitor cells ex vivo. Biomaterials [Internet]. Elsevier Ltd; 2009;30:2393–9. Available from: http://dx.doi.org/10.1016/j.biomaterials.2008.12.069
29. Carton F, Di Francesco D, Fusaro L, Zanella E, Apostolo C, Oltolina F, et al. Myogenic potential of extracellular matrix derived from decellularized bovine pericardium. Int J Mol Sci. 2021;22.
30. Brazile B, Lin S, Copeland KM, Butler JR, Cooley J, Brinkman-Ferguson E, et al. Ultrastructure and Biomechanics of Skeletal Muscle ECM. Bio-Instructive Scaffolds Musculoskelet Tissue Eng Regen

Med [Internet]. Elsevier; 2017. p. 139–60. Available from: http://dx.doi.org/10.1016/B978-0-12-803394-4.00006-9

31. Porzionato A, Sfriso MM, Pontini A, Macchi V, Petrelli L, Pavan PG, et al. Decellularized human skeletal muscle as biologic scaffold for reconstructive surgery. Int J Mol Sci. 2015;16:14808–31.
32. Jank BJ, Xiong L, Moser PT, Guyette JP, Ren X, Cetrulo CL, et al. Engineered composite tissue as a bioartificial limb graft. Biomaterials [Internet]. Elsevier Ltd; 2015;61:246–56. Available from: http://dx.doi.org/10.1016/j.biomaterials.2015.04.051
33. Urciuolo A, Urbani L, Perin S, Maghsoudlou P, Scottoni F, Gjinovci A, et al. Decellularised skeletal muscles allow functional muscle regeneration by promoting host cell migration. Sci Rep. 2018;8:1–20.
34. Hama H, Hioki H, Namiki K, Hoshida T, Kurokawa H, Ishidate F, et al. ScaleS: An optical clearing palette for biological imaging. Nat Neurosci. 2015;18:1518–29.
35. Schneider CA, Rasband WS, Eliceiri KW. NIH Image to ImageJ: 25 years of image analysis. Nat Methods [Internet]. London: Springer London; 2012;9:671–5. Available from: http://link.springer.com/10.1007/978-1-84882-087-6_9
36. Lee K Il, Lee JS, Kim JG, Kang KT, Jang JW, Shim YB, et al. Mechanical properties of decellularized tendon cultured by cyclic straining bioreactor. J Biomed Mater Res - Part A. 2013;101:3152–8.
37. Chaturvedi V, Dye DE, Kinnear BF, Van Kuppevelt TH, Grounds MD, Coombe DR. Interactions between skeletal muscle myoblasts and their extracellular matrix revealed by a serum free culture system. PLoS One. 2015;10:1–27.
38. Mattila PK, Lappalainen P. Filopodia: Molecular architecture and cellular functions. Nat Rev Mol Cell Biol. 2008;9:446–54.
39. Caswell PT, Zech T. Actin-Based Cell Protrusion in a 3D Matrix. Trends Cell Biol [Internet]. Elsevier Ltd; 2018;28:823–34. Available from: https://doi.org/10.1016/j.tcb.2018.06.003
40. Arnold HH, Braun T. 4 Genetics of Muscle Determination and Development. Curr Top Dev Biol. 1999;48:129–64.
41. Schmidt M, Schüler SC, Hüttner SS, von Eyss B, von Maltzahn J. Adult stem cells at work: regenerating skeletal muscle. Cell Mol Life Sci [Internet]. Springer International Publishing; 2019;76:2559–70. Available from: https://doi.org/10.1007/s00018-019-03093-6
42. Megeney LA, Rudnicki MA. Determination versus differentiation and the MyoD family of transcription factors. Biochem Cell Biol. 1995;73:723–32.
43. Ganassi M, Badodi S, Ortuste Quiroga HP, Zammit PS, Hinits Y, Hughes SM. Myogenin promotes myocyte fusion to balance fibre number and size. Nat Commun. 2018;9.
44. Wright WE, Sassoon DA, Lin VK. Myogenin, a factor regulating myogenesis, has a domain homologous to MyoD. Cell. 1989;56:607–17.
45. Agarwal M, Sharma A, Kumar P, Kumar A, Bharadwaj A, Saini M, et al. Myosin heavy chain-embryonic regulates skeletal muscle differentiation during mammalian development. Dev. 2020;147:1–14.

46. Biressi S, Molinaro M, Cossu G. Cellular heterogeneity during vertebrate skeletal muscle development. Dev Biol. 2007;308:281–93.
47. Schiaffino S, Reggiani C. Myosin isoforms in mammalian skeletal muscle. J Appl Physiol. 1994;77:493–501.
48. Jacquemet G, Hamidi H, Ivaska J. Filopodia in cell adhesion, 3D migration and cancer cell invasion. Curr Opin Cell Biol [Internet]. Elsevier Ltd; 2015;36:23–31. Available from: http://dx.doi.org/10.1016/j.ceb.2015.06.007
49. Flemming RG, Murphy CJ, Abrams GA, Goodman SL, Nealey PF. Effects of synthetic micro- and nano-structured surfaces on cell behavior. Biomaterials. 1999;20:573–88.
50. Vaz R, Martins GG, Thorsteinsdóttir S, Rodrigues G. Fibronectin promotes migration, alignment and fusion in an in vitro myoblast cell model. Cell Tissue Res. 2012;348:569–78.
51. Vandenburgh HH, Karlisch P, Farr L. Maintenance of highly contractile tissue-cultured avian skeletal myotubes in collagen gel. Vitr Cell Dev Biol [Internet]. 1988;24:166–74. Available from: http://link.springer.com/10.1007/BF02623542
52. Bettadapur A, Suh GC, Geisse NA, Wang ER, Hua C, Huber HA, et al. Prolonged Culture of Aligned Skeletal Myotubes on Micromolded Gelatin Hydrogels. Sci Rep [Internet]. Nature Publishing Group; 2016;6:1–14. Available from: http://dx.doi.org/10.1038/srep28855
53. Engler AJ, Griffin MA, Sen S, Bönnemann CG, Sweeney HL, Discher DE. Myotubes differentiate optimally on substrates with tissue-like stiffness: Pathological implications for soft or stiff microenvironments. J Cell Biol. 2004;166:877–87.
54. Sun Y, Duffy R, Lee A, Feinberg AW. Optimizing the structure and contractility of engineered skeletal muscle thin films. Acta Biomater [Internet]. Acta Materialia Inc.; 2013;9:7885–94. Available from: http://dx.doi.org/10.1016/j.actbio.2013.04.036
55. Duffy RM, Sun Y, Feinberg AW. Understanding the Role of ECM Protein Composition and Geometric Micropatterning for Engineering Human Skeletal Muscle. Ann Biomed Eng. 2016;44:2076–89.
56. Wang PY, Thissen H, Tsai WB. The roles of RGD and grooved topography in the adhesion, morphology, and differentiation of C2C12 skeletal myoblasts. Biotechnol Bioeng. 2012;109:2104–15.
57. Toral-Ojeda I, Aldanondo G, Lasa-Elgarresta J, Lasa-Fernandez H, Vesga-Castro C, Mouly V, et al. A Novel Functional In Vitro Model that Recapitulates Human Muscle Disorders. Muscle Cell Tissue - Curr Status Res F [Internet]. InTech; 2018. p. 13. Available from: https://www.intechopen.com/books/advanced-biometric-technologies/liveness-detection-in-biometrics
58. Guo X, Greene K, Akanda N, Smith AST, Stancescu M, Lambert S, et al. In vitro differentiation of functional human skeletal myotubes in a defined system. Biomater Sci. 2014;2:131–8.
59. Gillies AR, Smith LR, Lieber RL, Varghese S. Method for Decellularizing Skeletal Muscle Without Detergents or Proteolytic Enzymes. Tissue Eng Part C Methods [Internet]. 2011;17:383–9. Available from: http://www.liebertonline.com/doi/abs/10.1089/ten.tec.2010.0438

# Figures

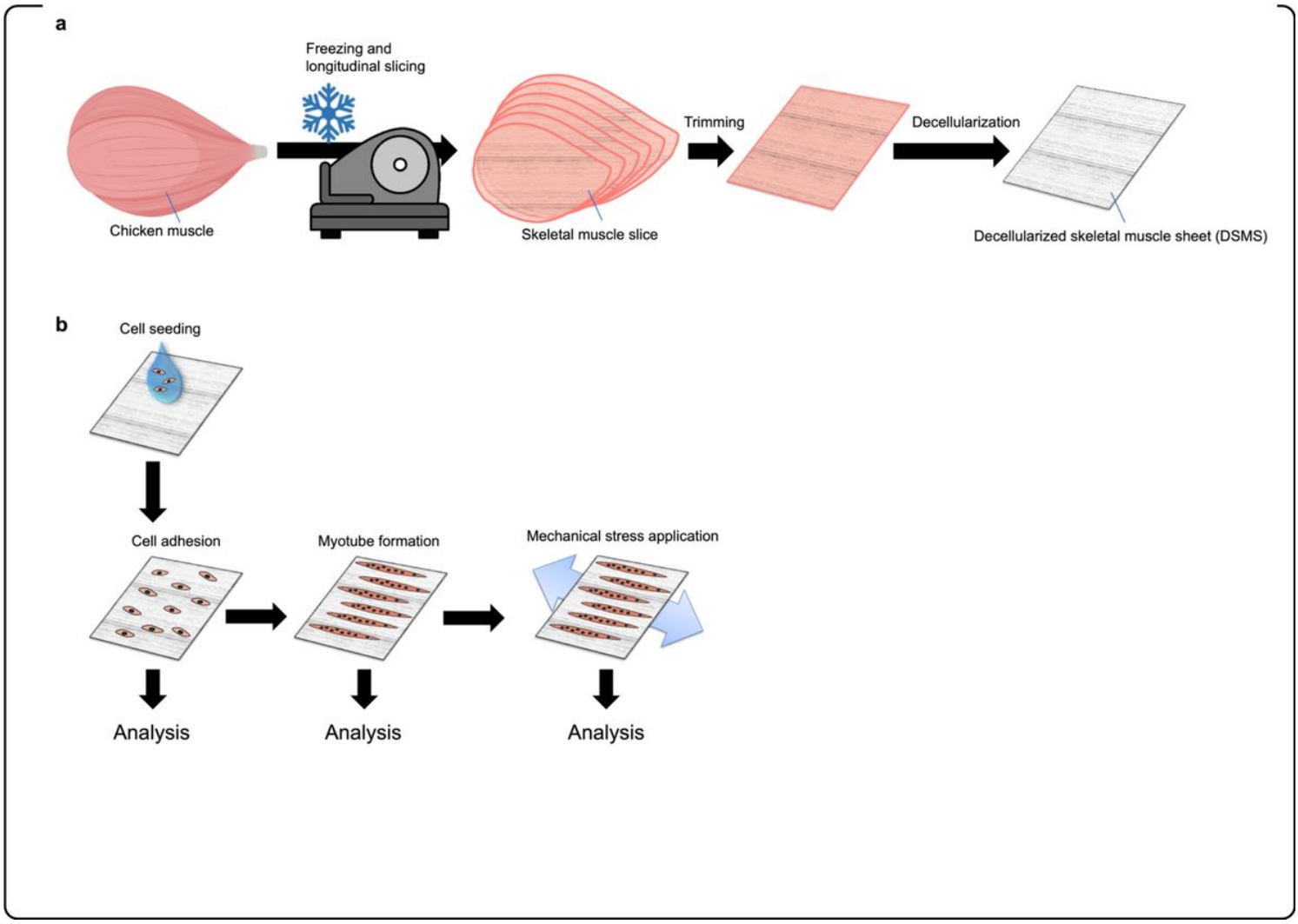


**Figure 1**

Schematic representation of the DSMS method. **a** Fabrication of decellularized skeletal muscle sheet. **b** Application of cell culture using DSMS.

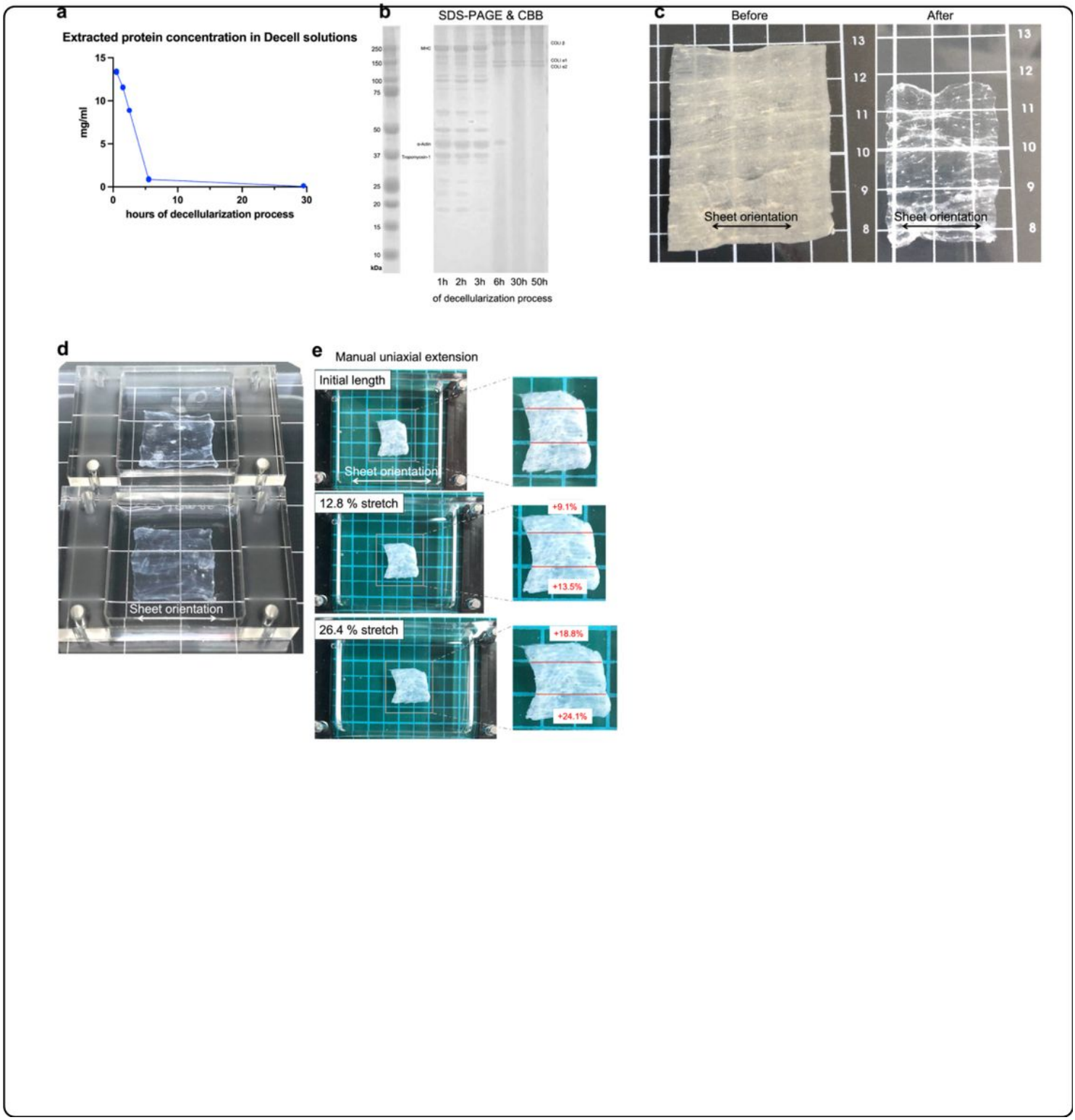


## Figure 2

Preparation and properties of decellularized skeletal muscle sheets. **a** Change in the amount of protein eluted by the decellularization solution. **b** Change in the remaining protein in the skeletal muscle sheet. The remaining protein was extracted and visualized by SDS-PAGE and CBB staining. **c** Appearance of the sheet before and after decellularization. DSMS: the direction of the ECM remaining in the sheets can be

visually confirmed. **d** DSMS attached to the chamber. **e** DSMS extension associated with manual stretching.

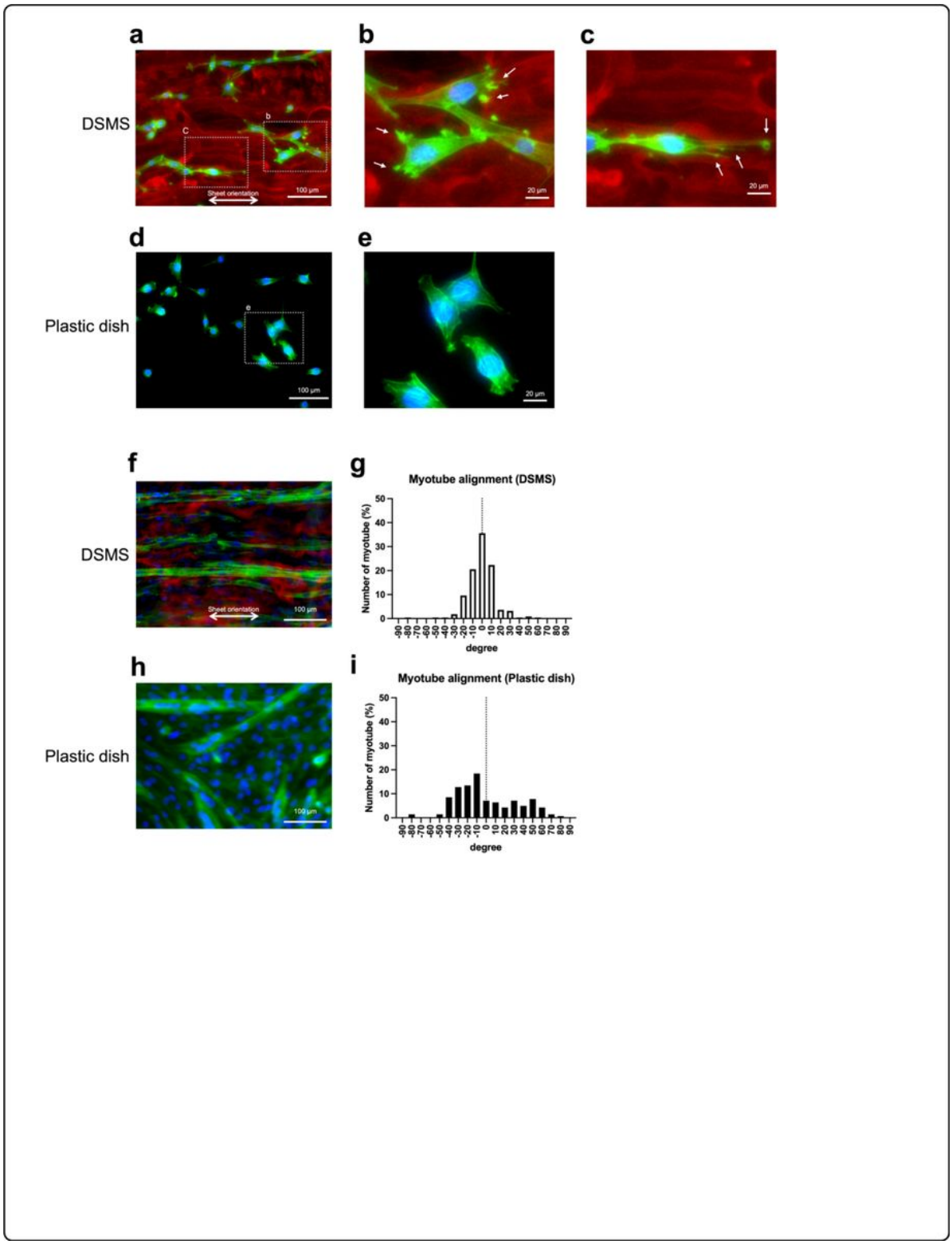


## Figure 3

Comparison of myoblasts and myotubes morphology. Green: phalloidin, red: COL IV, and blue: Hoechst 33342. **a** Myoblasts adhered to DSMS. Myoblasts aligned with the remaining COL IV in DSMS. **b:**

Magnified image. Myoblasts on DSMS developed actin spikes that appeared to be adhesion plaques (arrow). **c:** Magnified image. Myoblasts on DSMS developed lamellipodia and filipodia (arrow). **d** Myoblast adhered to the plastic dish. **e** Magnified image. Myoblasts on plastic dishes do not develop adhesive spots. **f** Myotube formation on DSMS. Myotube formed along with the ECM orientation in DSMS. **g** Histogram of angles in myotube formed on DSMS. Most myotubes were in the ± 20 ° range. **h** Myotube formation on the plastic plate. Myotube on a plastic formed in random orientation. **i** Histogram of angles in myotube formed on the plastic plate. Various angles of myotubes were present on the plastic plate.

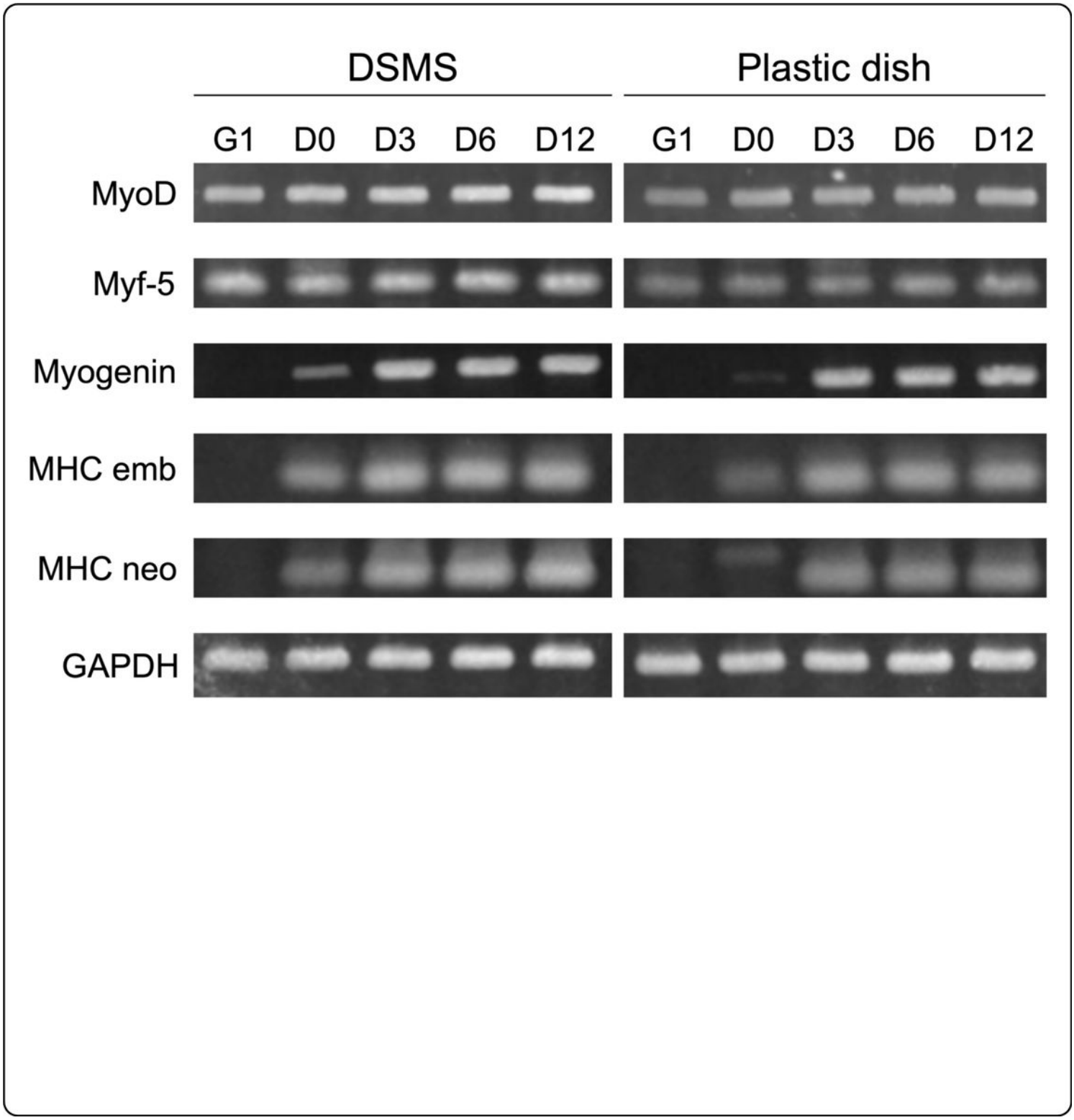


**Figure 4**

Semi-quantitative RT-PCR of gene expression involved in myocyte differentiation.

G1, Growth 1 day. D0–D12, differentiation 0–12 days. The numbers above the bands indicate the band intensities determined by densitometry. Each band intensity was corrected by the GAPDH band intensity value and then normalized by the DSMS G1 value.

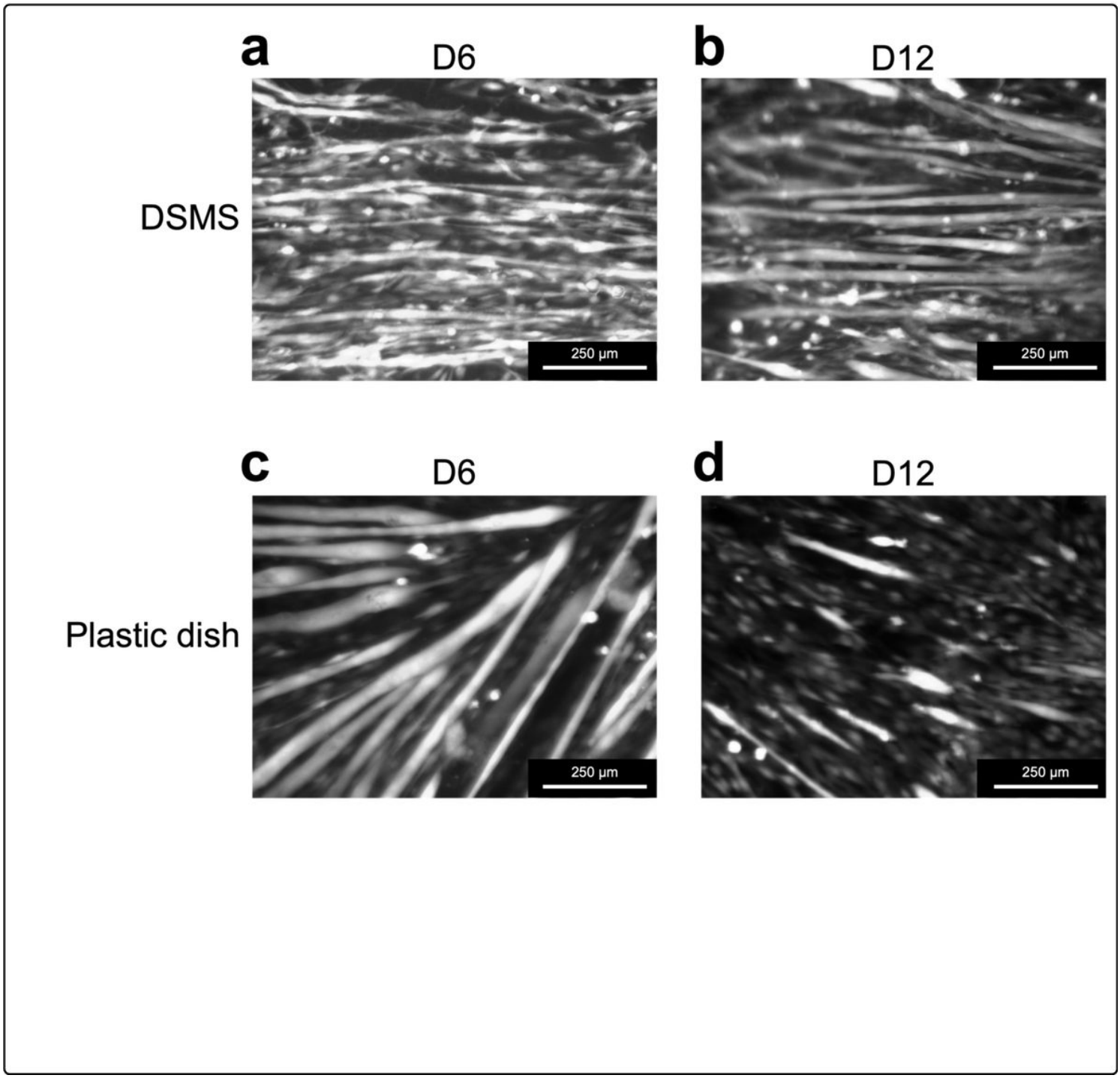


## Figure 5

Comparison of cell survival. Live cells were stained with calcein. **a, b** Live cells on DSMS. **c, d** Live cells on the plastic plate. **a, c** Differentiation 6 days. **b, d** Differentiation 12 days. In the culture on DSMS, detachment of myotubes was not observed even at 12 days of differentiation. In the culture on the plastic dish, myotubes were formed on Day 6 of differentiation, but many myotubes detached on Day 12.